Molecular Structure of the Oxidized High-Potential Iron–Sulfur Protein Isolated from *Ectothiorhodospira vacuolata*[†,‡]

Matthew M. Benning,[§] Terrance E. Meyer,[∥] Ivan Rayment,[§] and Hazel M. Holden*[,§]

Institute for Enzyme Research, Graduate School and Department of Biochemistry, University of Wisconsin, Madison, Wisconsin 53705, and Department of Biochemistry, University of Arizona, Tucson, Arizona 85721

Received September 22, 1993; Revised Manuscript Received December 1, 1993[⊗]

ABSTRACT: The high-potential iron–sulfur protein (iso-form II) isolated from *Ectothiorhodospira vacuolata* has been crystallized and its three-dimensional structure determined by molecular replacement procedures and refined to 1.8-Å resolution with a crystallographic R factor of 16.3%. Crystals employed in the investigation belonged to the space group $C222_1$ with unit cell dimensions of a = 58.4 Å, b = 64.7 Å, and c = 39.3 Å and one molecule per asymmetric unit. Like those HiPIPs structurally characterized thus far, the *E. vacuolata* molecule contains mostly reverse turns that wrap around the iron–sulfur cluster with cysteine residues 34, 37, 51, and 65 ligating the metal center to the polypeptide chain. There are 57 ordered solvent molecules, most of which lie at the surface of the protein. Two of these water molecules play important structural roles by stabilizing the loops located between Asp 42 and Lys 57. The metal center binding pocket is decidedly hydrophobic with the closest solvent molecule being 6.9 Å from S2 of the [4Fe-4S] cluster. The *E. vacuolata* HiPIP molecules pack in the crystalline lattice as dimers with their iron–sulfur centers approximately 17.5 Å apart. On the basis of biochemical properties, it was anticipated that the *E. vacuolata* HiPIP would be structurally more similar to the HiPIP isolated from *Ectothiorhodospira halophila* than to the protein obtained from *Chromatium vinosum*. In fact, the *E. vacuolata* molecule is as structurally close to the *C. vinosum* HiPIP as it is to the *E. halophila* protein due to the presence of various insertions and deletions that disrupt local folding. The *E. vacuolata* HiPIP structure thus calls into question whether molecular modeling experiments, based on primary structure homology alone, are valid when numerous insertions and deletions are present.

The high-potential iron–sulfur proteins (HiPIPs) are a group of low molecular weight electron transport proteins typically isolated from purple phototrophic bacteria (Bartsch, 1978). A key feature of these proteins is the presence of a [4Fe-4S] cluster which undergoes a reversible one-electron transfer reaction at a characteristically high oxidation–reduction midpoint potential of between +50 and +450 mV (Meyer *et al.*, 1983). The first three-dimensional structure of a HiPIP, namely, that isolated from *Chromatium vinosum*, was determined nearly 20 years ago in the laboratory of Dr. Joseph Kraut (Carter *et al.*, 1974; Freer *et al.*, 1975). From that elegant X-ray investigation, it was shown that the secondary structure of the *C. vinosum* HiPIP consists of two short α-helical segments, three strands of antiparallel β-pleated sheet, and various reverse turns that wrap around to bury the [4Fe-4S] center within the protein matrix. In addition, the X-ray analysis demonstrated that the irons and inorganic sulfurs of the prosthetic group adopt a cubane-type configuration as also observed in the three-dimensional structure of the low-potential bacterial ferredoxin isolated from *Peptococcus aerogenes* (Adman *et al.*, 1973, 1976). Unlike the HiPIPs, however, the low-potential ferredoxins contain two such clusters per polypeptide chain and transfer electrons at low redox potentials near −400 mV (Stombaugh *et al.*, 1976).

When the three-dimensional structures of the reduced *C. vinosum* HiPIP and the oxidized *P. aerogenes* ferredoxin were subsequently compared, the iron–sulfur clusters appeared to be indistinguishable (Carter *et al.*, 1972). From this comparison, the so-called "three-state" hypothesis was set forth to reconcile the vastly differing magnetic properties and redox potentials displayed by these two proteins (Carter *et al.*, 1972). The main premise of the theory was that three oxidation states are available to the [4Fe-4S] cluster with overall net charges of −1, −2, and −3 when attached to a protein via cysteinyl ligands. The HiPIPs transfer electrons between the −1 and −2 states, whereas the low-potential ferredoxins utilize the −2 and −3 states. The HiPIPs and ferredoxins thus share in common the −2 state which is EPR silent.

Prior to the proposal of Carter *et al.* (1972), the synthetic analog $(Et_4N)_2[Fe_4S_4(SCH_2Ph)_4]$ was prepared and chemically characterized, and its X-ray structure was determined by Herskovitz *et al.* (1972). On the basis of proton magnetic resonance, Mössbauer, photoelectron, and electronic spectra, and magnetic susceptibility, the authors concluded that the oxidation states of the synthetic analog, the reduced form of the HiPIP, and the oxidized form the low-potential bacterial ferredoxin were equivalent, thus lending further evidence in support of the "three-state" hypothesis.

The factors that determine which oxidation states are available to the metal center when associated with a protein are still being investigated and are subject to much speculation. It has been suggested, for example, that the extent of hydrogen

[†] This research was supported in part by grants from the NIH (GM30982 to H.M.H. and GM21277 to T.E.M.). H.M.H. is an Established Investigator of the American Heart Association.

[‡] X-ray coordinates for the *E. vacuolata* HiPIP have been deposited in the Brookhaven Protein Data Bank (accession no. 1HPI; (Bernstein *et al.*, 1977) or may be obtained immediately via HOLDEN@ENZYME.WISC.EDU.

* To whom correspondence should be addressed.

[§] University of Wisconsin—Madison.

[∥] University of Arizona.

[⊗] Abstract published in *Advance ACS Abstracts,* February 15, 1994.

0006-2960/94/0433-2476$04.50/0

Table 1: Intensity Statistics for the Native X-ray Data Set

	resolution range (Å)								
	overall	29.2–5.09	–3.60	–2.94	–2.55	–2.28	–2.08	–1.92	–1.80
no. of measurements	19816	876	2528	3082	3416	3234	2588	2174	1918
no. of independent reflections[a]	7028	316 (224)	629 (603)	788 (759)	936 (899)	1013 (933)	1090 (692)	1122 (451)	1134 (439)
% of the theoretical no. of reflections	98	87	100	99	100	100	99	89	93
average intensity		2001	2299	1327	615	564	472	259	191
sigma		87	86	55	35	40	38	28	27
R_{factor} (%)[b]	4.9	2.1	2.2	2.7	4.0	4.8	5.3	7.3	9.5

[a] This is the number of reduced observations. Shown in parentheses is the number of independent measurements for which there were not duplicate or symmetry related observations. [b] $R_{factor} = \Sigma|I - \bar{I}|/\Sigma I \times 100$.

bonding to the metal cluster plays a critical role in this regard (Adman *et al.*, 1975). Other factors thought to modulate the oxidation–reduction potentials of the [4Fe-4S] cluster include protein flexibility, solvent accessibility of the cluster, number and positions of hydrophobic residues surrounding the metal center, and the electrostatic field of the protein.

Within recent years there has been a resurgence of structure/function research interest in the HiPIPs due in part to the significant variation in their amino acid sequences, molecular sizes, overall net charges, and redox potentials. For example, the X-ray structures of two other HiPIPs, namely, those isolated from *Rhodocyclus tenuis* and *Ectothiorhodospira halophila* (isoform-I), have now been determined to high resolution and have been shown to display significant similarities and differences with respect to the *C. vinosum* molecule (Rayment *et al.*, 1992; Breiter *et al.*, 1991). Additionally, the HiPIPs have been the focus of various NMR studies including the recent investigation of the *E. halophila* (isoform-II) protein (Banci *et al.*, 1993). Theoretical investigations have also been conducted on the low-potential ferredoxins and the *C. vinosum* HiPIP in an attempt to further correlate the relationship between the three-dimensional architecture of the protein and the redox potential of its iron–sulfur cluster (Langen *et al.*, 1992). While the [4Fe-4S] cluster is ubiquitous in nature and is found in more complicated protein systems such as aconitase, NADH dehydrogenase, sulfite reductase, and nitrogenase [for a review, see Beinert (1990)], the HiPIPs present distinct advantages for such structure/function studies in that they are small and when crystals are obtained they generally diffract to high resolution thereby yielding very accurately determined protein structures.

Here we report the crystallization, structure determination, and least-squares refinement to 1.8-Å resolution of the HiPIP isolated from *Ectothiorhodospira vacuolata* (isoform-II). This particular HiPIP was chosen for study because its molecular size, amino acid sequence, and redox potential are similar to those of the *E. halophila* protein whose high-resolution X-ray structure is known (Ambler *et al.*, 1994; Holden, unpublished results). As will be described, the molecular motif exhibited by the *E. vacuolata* HiPIP provides several interesting surprises and, indeed, calls into question whether molecular modeling experiments, based on primary structure homology alone, are valid for this class of proteins.

MATERIALS AND METHODS

Crystallization. Two isoforms of the HiPIP from *E. vacuolata* strain β1 (DSM 2111) were isolated and purified according to the procedures of Kusche and Truper (1984) and Bartsch (1978). Small, thin, diamond-shaped crystals of the *E. vacuolata* (isoform-II) HiPIP were obtained by vapor diffusion against 2.2 M ammonium sulfate, 50 mM Na^+/K^+ phosphate, and 5 mM NaN_3, pH 7.0, at room temperature and in the presence of atmospheric oxygen. For these experiments, the protein concentration was typically 20–40 mg/mL. To grow larger, single crystals, the technique of macroseeding was employed (Thaller *et al.*, 1981, 1985). For such experiments, 10 μL of protein was mixed with 10 μL of 1.7 M ammonium sulfate, 50 mM Na^+/K^+ phosphate, and 5 mM NaN_3, pH 7.0, and equilibrated in hanging drops against either 1.7 or 1.8 M ammonium sulfate buffered at the same pH for 6 days. Single diamond-shaped seeds grown from 2.2 M ammonium sulfate were washed in 1.5 M ammonium sulfate and subsequently transferred to the hanging drops. The seeds grew over a period of approximately 6 weeks and attained typical dimensions of 0.5 mm × 0.5 mm × 0.2 mm. No attempts were made to keep the crystals in the oxidized state, although due to the low potential of the *E. vacuolata* HiPIP, the oxidized form is stable in the presence of atmospheric oxygen.

Using precession photography, the crystals were shown to belong to the space group $C222_1$ with unit cell dimensions of a = 58.4 Å, b = 64.7 Å, and c = 39.3 Å and one molecule per asymmetric unit. The Matthews coefficient, (V_m), for these crystals was 2.3 Å^3/Dalton, thus corresponding to a solvent content of approximately 47% (Matthews, 1968). The crystals diffracted to a nominal resolution of 1.8 Å.

X-ray Data Collection and Processing. For X-ray data collection, crystals were mounted in quartz capillary tubes. To prevent slippage, the crystals were covered with small volumes of a solution containing 0.2% poly(vinylformal) dissolved in 1,2-dichloroethane (Rayment *et al.*, 1977). A native X-ray data set was collected to 1.8-Å resolution from a single crystal at 4 °C with a Siemens X1000D area detector system. The X-ray source was nickel-filtered copper Kα radiation from a Rigaku RU200 X-ray generator operated at 50 kV and 50 mA. These X-ray data were subsequently processed with the data reduction software package XDS (Kabsch, 1988a,b) and internally scaled according to the algorithm of Fox and Holmes (1966) as implemented by Dr. Phil Evans. Relevant X-ray data collection statistics may be found in Table 1. The native X-ray data set was 97% complete to 1.8-Å resolution.

Structure Determination and Least-Squares Refinement. Initial protein phases were determined by molecular replacement techniques with the software package MERLOT (Fitzgerald, 1988). On the basis of the amino acid sequence for the *E. vacuolata* HiPIP (Ambler *et al.*, 1994), a search model, with nonconserved amino acid residues truncated to alanines, was constructed from the known three-dimensional model of the *E. halophila* (isoform-I) HiPIP structure (Breiter *et al.*, 1991). Structure factors for this search model were calculated by placing the truncated *E. halophila* HiPIP into a cubic unit cell with $P1$ symmetry and unit cell dimensions of 150 Å. Cross rotation function maps were calculated by

Table 2: Refinement Statistics

resolution limits (Å)	30–1.8
R factor (%)[a]	16.3
no. of reflections used	6973
no. of protein atoms	556
no. of solvent molecules	57
weighted root-mean-square deviations from ideality	
bond length (Å)	0.007
bond angle (deg)	2.2
planarity (trigonal) (Å)	0.004
planarity (other planes) (Å)	0.006
torsion angle (deg)[b]	15.6

[a] R factor = $\Sigma|F_o - F_c|/\Sigma|F_o|$. [b] The torsion angles were not restrained during the refinement.

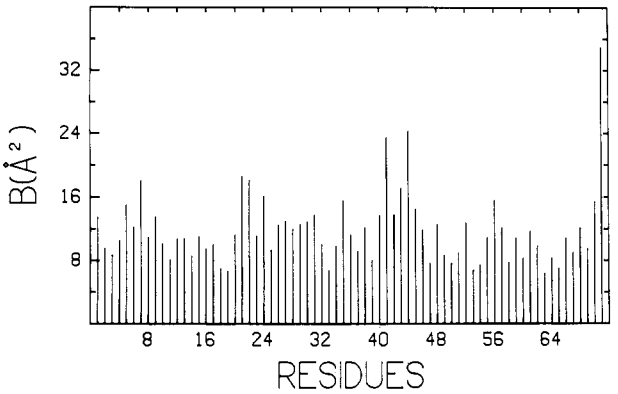

FIGURE 1: Plot of the mean main-chain temperature factors versus amino acid residue number. As can be seen, the backbone atoms have very low temperature factors. Only six side chains (Asp 8, Arg 17, Gln 24, Glu 29, Glu 30, Lys 57) have high B values.

the technique of Crowther (1972) within a resolution range of 10.0–4.0 Å and a Patterson search radius of 15 Å. A peak corresponding to the Eulerian angles of $\alpha = 35.0$, $\beta = 143.0$, and $\gamma = 50.0$ appeared at 7σ and was the largest feature in the map. Based on these angles, the search model was rotated and a solution to the translation problem was subsequently determined by an R factor search. At the position $x = 0.08$, $y = 0.03$, and $z = 0.06$, the R factor dropped to 48%.

From the results of the rotational and translational searches, a preliminary chain tracing of the *E. vacuolata* HiPIP was constructed by including all those amino acid residues that had been truncated in the search model and subsequently subjected to alternate cycles of least-squares refinement and model building with the software packages TNT and FRODO, respectively (Tronrud *et al.*, 1987; Jones, 1985). Ideal stereochemistry for the [4Fe-4S] cluster was based on the small molecule structure determination of $Fe_4(NO)_4(\mu_3\text{-}S)_4$ (Chu *et al.*, 1982). During the last cycles of refinement, the metal cluster geometry was not restrained. Small peaks of electron density located within 3.5 Å of potential hydrogen-bonding groups were modeled as water molecules. A total of 57 solvent molecules was included in the refinement. The average temperature factor for the solvent was 29 Å^2 with 31 of the water molecules having temperature factors below 30 Å^2. The final R factor for the *E. vacuolata* model was 16.3% for all measured X-ray data from 30.0–1.8-Å resolution. Relevant least-squares refinement statistics may be found in Table 2. A plot of the mean main-chain temperature factors is given in Figure 1, and a Ramachandran plot of all non-glycinyl residues is shown in Figure 2. The average temperature factor for all backbone atoms was 11 Å^2. A representative portion of the electron density map is displayed in Figure 3. The electron density was very well-ordered except for the following side chains: the carboxylate group of Asp 8, the guanido group of Arg 17, the side chain amide group of Gln 24, the carboxylate group of Glu 29, $O^{\delta 2}$ of Glu 30, and N^{ζ} of Lys 57.

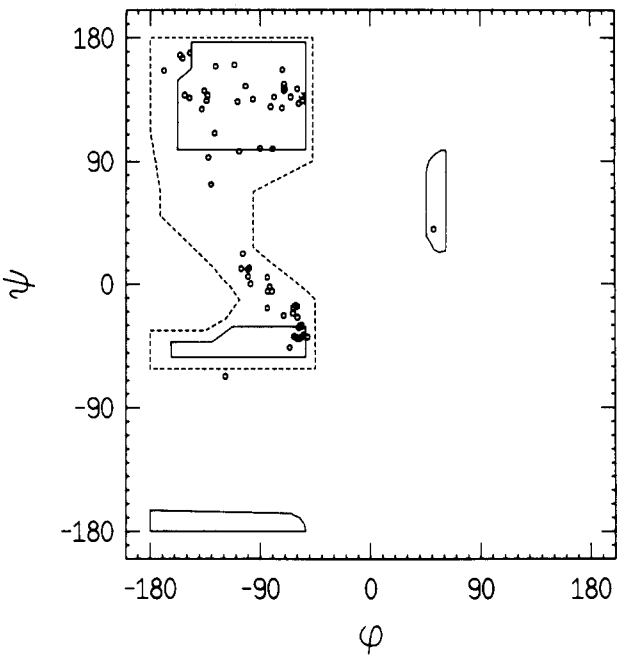

FIGURE 2: ϕ,ψ plot of all non-glycinyl main-chain dihedral angles. Fully allowed ϕ,ψ values are enclosed by solid lines; those only partially allowed are enclosed by dashed lines. There is only one outlier (Asp 47). As can be seen, the *E. vacuolata* HiPIP contains very little secondary structure with respect to α-helices and β-pleated sheets.

RESULTS AND DISCUSSION

With respect to primary structures, the *E. halophila* (isoform-I) and *E. vacuolata* (isoform-II) HiPIPs contain 71 amino acid residues each and show an overall amino acid sequence identity of 34% (Ambler *et al.*, 1994). Both the *E. halophila* and the *E. vacuolata* proteins are similar with respect to overall net charges (–11 and –8) and redox potentials (+120 and +150 mV) (Ambler *et al.*, 1994). On the basis of amino acid sequence alignments, it was expected that the *E. vacuolata* HiPIP model determined here would be more similar to that of the *E. halophila* protein than to the structure of the *C. vinosum* HiPIP which has a redox potential of +360 mV, an overall net charge of –4, and a total of 85 amino acid residues (Meyer *et al.*, 1983).

A ribbon representation of the *E. vacuolata* HiPIP is shown in Figure 4. Like those HiPIPs structurally characterized thus far, the *E. vacuolata* molecule contains mostly reverse turns that wrap around the iron–sulfur cluster with cysteine residues 34, 37, 51, and 65 ligating the metal center to the polypeptide chain. There are eight type I, two type II, and two type III turns. A list of the dihedral angles for these β-turns is given in Table 3. There is also one α-helix formed by residues Pro 9 to Ala 13.

A superposition of the *E. vacuolata* and *E. halophila* HiPIP models is given in Figure 5. According to the algorithm of Rossmann and Argos (1975), the α-carbons for these two proteins superimpose with a root-mean-square deviation of 0.68 Å for 55 structurally equivalent atoms, thus corresponding to a 77% three-dimensional identity. As can be seen from Figure 5, there are several noticeable differences in their molecular motifs, however. In the *E. vacuolata* structure there is a well-defined α-helix which is missing in the *E. halophila* protein. On the basis of amino acid sequence alignments and other biochemical considerations, it was

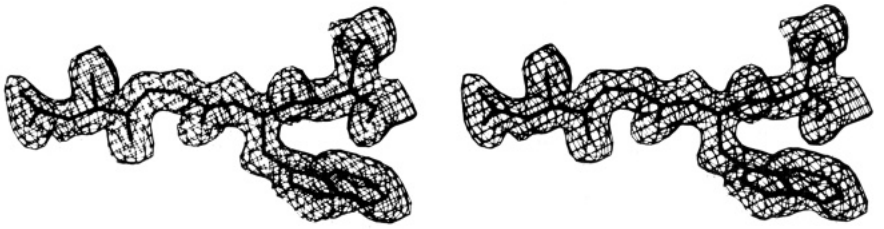

FIGURE 3: Representative portion of the electron density map calculated to 1.8-Å resolution. The electron density shown was calculated with coefficients of the form $(2F_o - F_c)$ and contoured at 1σ. This region corresponds to residues Asn 62, Gly 63, Trp 64, and Cys 65.

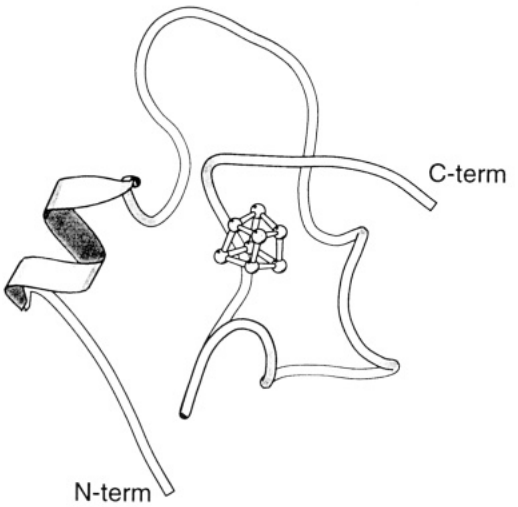

FIGURE 4: Ribbon representation of the *E. vacuolata* HiPIP. This figure was prepared with the software package MOLSCRIPT (Kraulis, 1991).

Table 3: Dihedral Angles for Reverse Turns

amino acid residue no.	type of turn	ϕ_2	ψ_2	ϕ_3	ψ_3
Ser 5–Asp 8	I	−63.0	−21.4	−99.8	10.6
Gln 12–Glu 15	I	−58.2	−31.7	−105.3	11.2
Asp 19–Ser 22	III	−57.5	−30.5	−59.7	−16.3
His 25–Tyr 28	I	−56.3	−30.9	−84.0	−17.6
Glu 29–Gln 32	II	−58.6	132.0	111.8	−17.8
Thr 33–Asn 36	III	−60.2	−39.1	−51.1	−38.6
Cys 37–Tyr 40	I	−56.1	−30.1	−80.2	−5.3
Asp 42–Ala 45	I	−61.0	−15.7	−97.6	0.1
Cys 51–Phe 54	I	−56.2	−31.0	−83.7	−5.3
Phe 54–Lys 57	II	−56.1	137.8	80.0	2.8
Ser 60–Gly 63	I	−59.3	−24.4	−98.8	11.8
Cys 65–Trp 68	I	−62.8	−17.4	−84.0	4.8

anticipated that this α-helix would be missing in the *E. vacuolata* protein. Also, from Figure 5, it can be seen that the loop delineated by Asp 42 to Asp 47 (*E. vacuolata* numbering) adopts quite different conformations in the two proteins although there is no indication from the amino acid sequences that this would be the case. The sequence for this loop is Asp 42, Ala 43, Ser 44, Ala 45, Gln 46, and Asp 47 in the *E. vacuolata* protein and Glu 39, Ala 40, Val 41, Gln 42, Asp 43, and Gly 44 in the *E. halophila* HiPIP. A superposition of the α-carbons for the *E. vacuolata* and *C. vinosum* molecules is displayed in Figure 6. The *E. vacuolata* and *C. vinosum* molecules exhibit a 75% three-dimensional structural identity and superimpose with a root-mean-square value of 0.46 Å for 53 equivalent α-carbons. Note that the N-terminal helix is present in both of these HiPIPs. To complete the comparisons, the *C. vinosum* and *E. halophila* HiPIP α-carbon positions superimpose with a root-mean-square deviation of 0.71 Å for 48 structurally equivalent atoms.

Excluding the four cysteinyl ligands, only two amino acid residues, Tyr 16 and Gly 63 (*E. vacuolata* numbering), are structurally conserved between the *C. vinosum*, *E. halophila*, *R. tenuis*, and the *E. vacuolata* HiPIPs. The conserved tyrosine has been thought to play a role in the modulation of redox potentials by interacting with one of the inorganic sulfur atoms of the metal cluster (Carter *et al.*, 1974). Its side chain O^{η} in the *E. vacuolata*, *C. vinosum*, *E. halophila*, and *R. tenuis* proteins is 4.9, 4.6, 4.7, and 4.4 Å, respectively, from the corresponding above-mentioned glycine α-carbon, suggesting a structural reason for the conservation of the glycine. Since the redox potentials for the HiPIPs from *C. vinosum*, *R. tenuis*, *E. vacuolata* (isoform-II), and *E. halophila* (isoform-I) are 360, 330, 150, and 120 mV, respectively, it is instructive to compare the distances between the conserved tyrosines and the iron–sulfur centers. In each case, $C^{\epsilon 2}$ of the tyrosine side chain approaches most closely S3 of the [4Fe-4S] cluster. For the *C. vinosum*, *R. tenuis*, *E. vacuolata*, and *E. halophila* HiPIPs, the distances between $C^{\epsilon 2}$ and S3 are 3.75, 3.80, 3.85, and 3.97 Å, respectively. While it appears that the distance between the tyrosine and the metal cluster

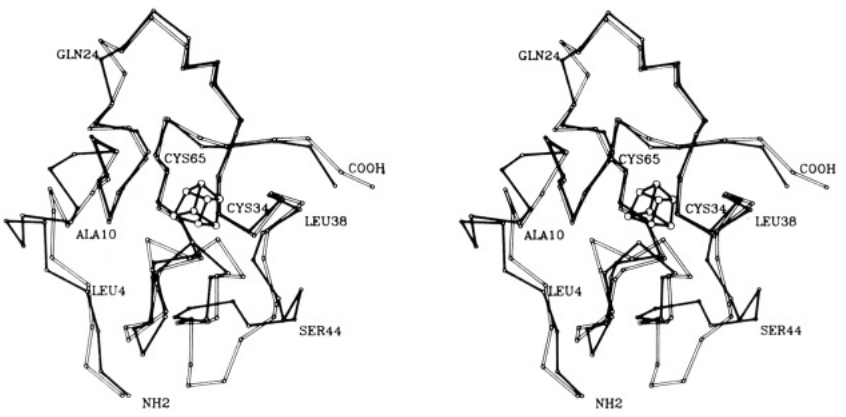

FIGURE 5: Superposition of the *E. vacuolata* and *E. halophila* HiPIPs. The α-carbons were superimposed according to the algorithm of Rossmann and Argos (1975). The *E. vacuolata* molecule is shown in closed bonds while the *E. halophila* protein is displayed in open bonds. The numbering corresponds to the *E. vacuolata* HiPIP.

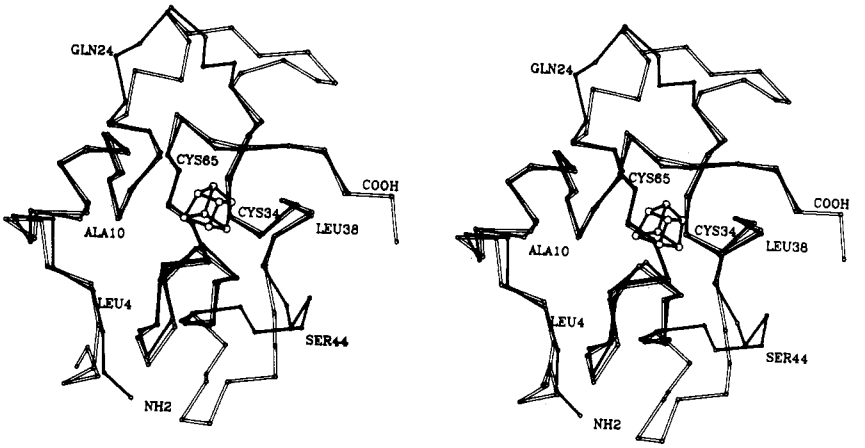

FIGURE 6: Superposition of the *E. vacuolata* and the *C. vinosum* HiPIPs. The *E. vacuolata* HiPIP is shown in closed bonds while the *C. vinosum* molecule is depicted in open bonds. The numbering corresponds to the *E. vacuolata* HiPIP. X-ray coordinates for the *C. vinosum* HiPIP were obtained from the Brookhaven Protein Data Bank (Bernstein *et al.*, 1977).

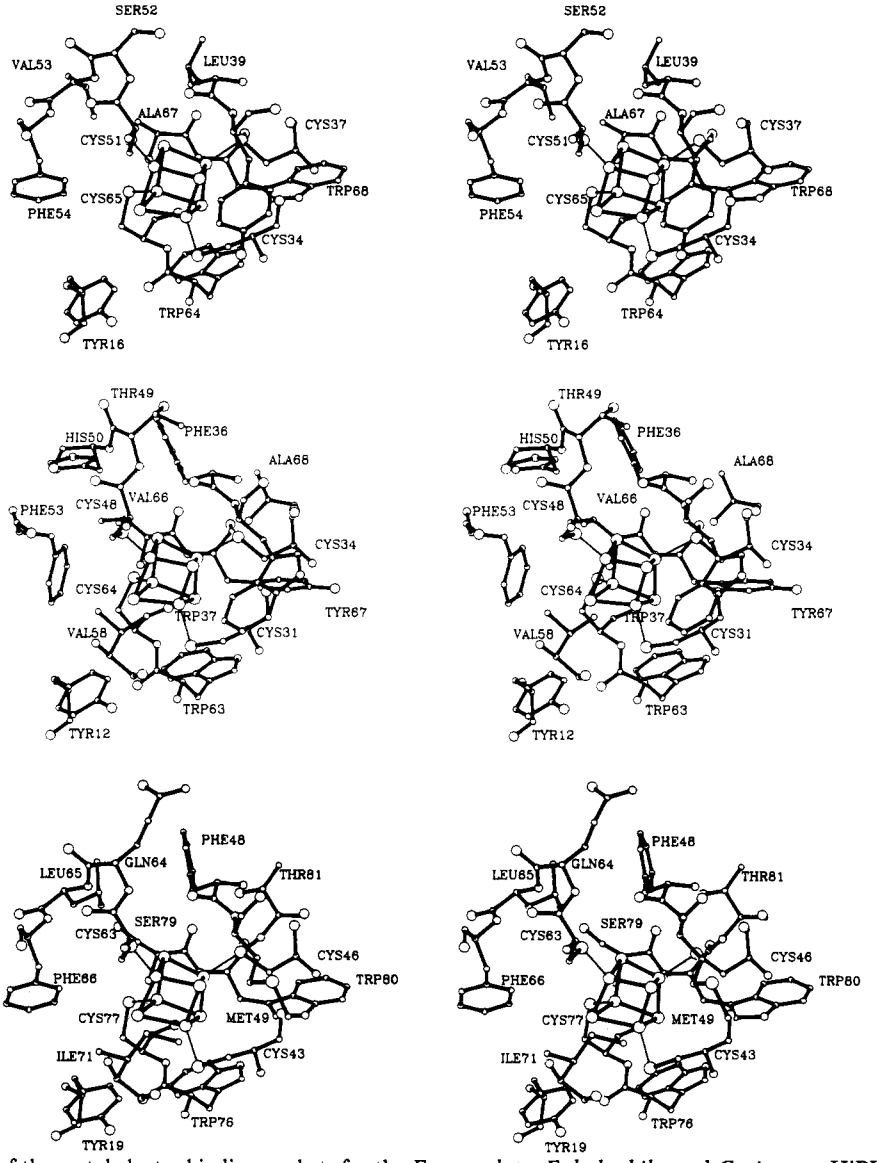

FIGURE 7: Close-up views of the metal cluster binding pockets for the *E. vacuolata*, *E. halophila*, and *C. vinosum* HiPIPs. Those amino acid residues that are within approximately 4.0 Å from the atoms of the cluster are shown for each of the HiPIPs. (a, top) *E. vacuolata* HiPIP. (b, middle) *E. halophila* HiPIP. (c, bottom) *C. vinosum* HiPIP.

increases with decreasing redox potential, the observed differences, within coordinate error, are not statistically significant. It is also possible that the tyrosine residue is conserved for some other biochemical function.

Close-up views of the metal center binding pockets for the *E. vacuolata*, *E. halophila*, and *C. vinosum* HiPIPs may be found in Figure 7a–c. When the *E. halophila* HiPIP structure was initially determined, it was observed that Phe 53 adopted

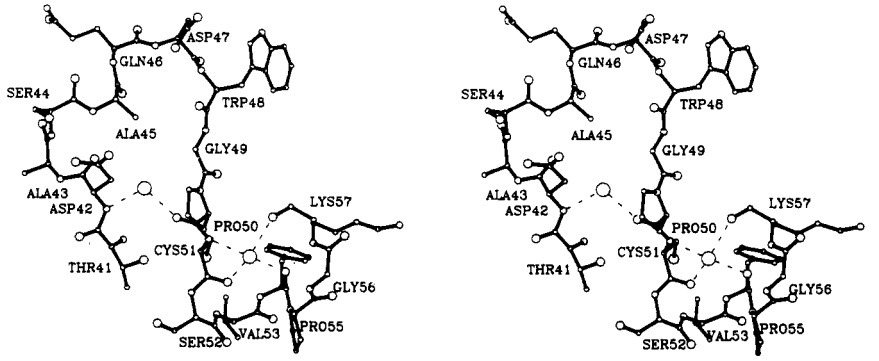

FIGURE 8: Protein environment of solvent molecules Sol O13 and Sol O15. The solvent molecules are displayed as spheres. Potential hydrogen bonds, ranging in length from 2.6 to 3.1 Å, are indicated by the dashed lines.

a quite different orientation with respect to the [4Fe-4S] cluster as compared to the structurally conserved Phe 66 in the *C. vinosum* HiPIP (Figure 7, panels b and c, respectively). Since these two HiPIPs display such differing redox potentials, it was suggested that perhaps the conformation of this aromatic group was important (Breiter *et al.*, 1991). Consequently, it was anticipated that the structurally similar Phe 54 in the *E. vacuolata* HiPIP would adopt the conformation as observed in the *E. halophila* protein. As can been seen in Figure 7a,b, however, this is not the case. There also appears to be no correlation between the number and positions of aromatic side chains surrounding the metal prosthetic group and the corresponding redox potentials. With respect to the hydrogen-bonding patterns, the *E. vacuolata* HiPIP displays the typical electrostatic interactions observed in the other HiPIPs whose structures are now known to high resolution. Specifically, there are four putative hydrogen bonds from backbone amide groups to the sulfurs of the cysteine ligands (Val 69–Cys 37, Leu 39–Cys 37, Val 53–Cys 51, and Ala 67–Cys 65) and one rather nonlinear interaction between the amide hydrogen of Cys 65 and the inorganic sulfur of the cluster. These interactions range in length from 3.3 to 3.6 Å.

In the oxidized form of the HiPIP, there are formally three Fe(III) ions, one Fe(II) ion, and four inorganic sulfides while in the reduced state there are two Fe(III) ions and two Fe(II) ions. In the small molecule structure determination of the compound $(Et_4N)_2[Fe_4S_4(SCH_2Ph)_4]$ by Herskovitz *et al.* (1972), it was concluded that a fully delocalized electronic description of the metal center was more appropriate than assigning formal oxidation states to each ion in the cluster. Recent NMR studies of the *E. halophila* (isoform-II) HiPIP, however, suggest that a more accurate description of the oxidation states of the irons is two iron (III) ions and a mixed valence iron(III)–iron(II) pair (Banci *et al.*, 1993). From these studies it was concluded that the iron ions participating in the mixed valence pair depend upon which HiPIP is being studied. On the basis of our X-ray coordinates determined at 2.5-Å resolution for the *E. halophila* HiPIP (isoform-I), Banci *et al.* concluded that the observed Fe–SCys bond distances (ranging from 2.02 to 2.41 Å) further supported their conclusions that the iron ion ligated to "Cys 46" participates in the mixed valence pair in the *E. halophila* HiPIP (isoform-II). However, these distances were based on a structure determined at 2.5-Å resolution and were quoted for only one of the molecules in the crystalline asymmetric unit. Table 4 presents the Fe–SCys bond distances for the X-ray structures of the *R. tenuis*, *E. halophila*, and *E. vacuolata* HiPIPs, all of which have now been refined to 1.8-Å resolution or better in our laboratory. It should be emphasized that the cluster geometry was not restrained during the last cycles of refinement and model building. As can be seen,

Table 4: Iron–Cysteinyl Sulfur Bond Distances in HiPIPs (Å)

cysteine residue[a]	*R. tenuis* molecule I	*R. tenuis* molecule II	*E. halophila* molecule I	*E. halophila* molecule II	*E. vacuolata*
22	2.26	2.23	2.27	2.26	2.25
25	2.31	2.33	2.24	2.27	2.22
40	2.13	2.19	2.26	2.33	2.21
55	2.18	2.33	2.27	2.20	2.21

[a] Refers to the *R. tenuis* numbering.

there are no significant differences, within the limitations of X-ray coordinate errors, between the various iron–sulfur bond lengths. Note that the *R. tenuis* HiPIP structure was determined in the reduced form, whereas the *E. halophila* and *E. vacuolata* HiPIP structures were solved in the oxidized state. While the bond lengths observed in the X-ray structures do not rule out the "mixed" valence state, they also cannot be used to support it as was suggested by Banci *et al.* (1993).

Recent theoretical studies involving the low- and high-potential bacterial ferredoxins have suggested that redox potentials may be modulated in part by varying the solvent accessibility of the iron-sulfur cluster (Langen *et al.*, 1992). In the *E. vacuolata* HiPIP structure, there are 57 ordered solvent molecules that have been located in the electron density map. Of these, 14 serve to bridge different HiPIP molecules within the crystalline lattice, three of which have *B* values below 10.3 Å^2. In addition, there are two water molecules, labeled Sol O13 and Sol O15 in the X-ray coordinate set, with temperature factors below 10 Å^2. These particular solvent molecules serve to stabilize the region delineated by amino acid residues Asp 42–Lys 57 by forming hydrogen bonds between main-chain carbonyl and amide groups and are shown in Figure 8. On the basis of hydrogen-bonding patterns, none of these solvent molecules with low temperature factors appear to be cations.

The closest solvent molecule to the iron–sulfur center in the *E. vacuolata* HiPIP is Sol O13 and is located approximately 6.9 Å from S2 of the metal center. In the *E. halophila*, *R. tenuis*, and *C. vinosum* HiPIPs, the closest solvent molecules to the [4Fe-4S] clusters are located approximately 6.7, 6.0, and 7.5 Å from the centers, respectively. These distances suggest that structurally ordered solvent molecules may play only a small role in the modulation of redox potentials in the HiPIPs, although transient differences in solvent accessibilities cannot be ruled out as a possible mechanism of redox potential control.

According to their behavior on gel filtration columns, it was originally assumed that HiPIPs function as monomers *in vivo*. Recent isolation of a HiPIP from the purple phototrophic bacterium *Rhodospirillum salinarum*, however, has shown

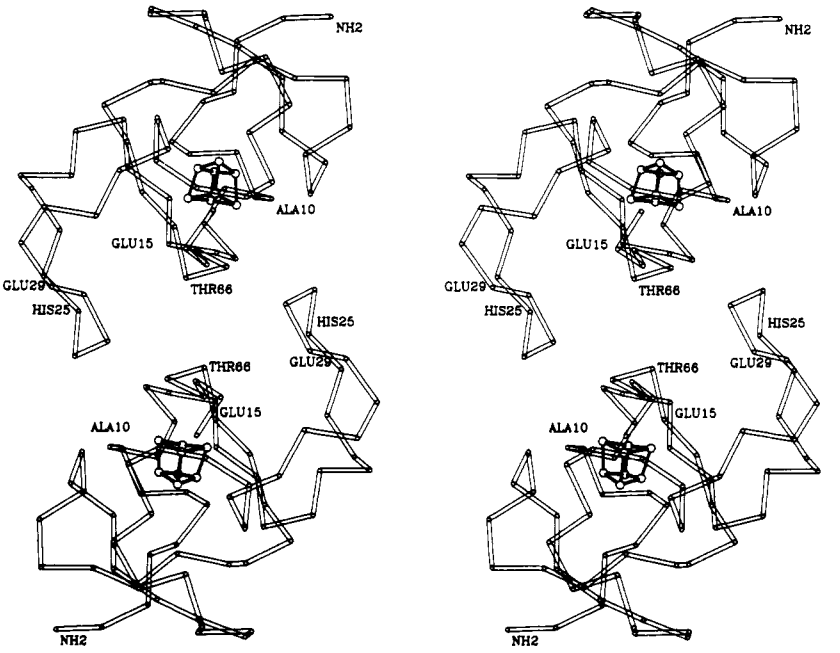

FIGURE 9: Crystallographic dimer of the *E. vacuolata* HiPIP. The figure is oriented such that the crystallographic 2-fold rotation axis is perpendicular to the plane of the paper.

that this protein exists as either a tetramer or hexamer (Meyer *et al.*, 1990). In addition, EPR studies of Dunham *et al.* (1991) have demonstrated that freezing the *C. vinosum* HiPIP in the presence of 0.1–2.0 M NaCl induces aggregation of monomers to dimers. Both the *E. halophila* and the *R. tenuis* HiPIPs crystallize with two molecules per asymmetric unit, and, indeed, they aggregate in the crystalline lattice as dimers with approximate local 2-fold rotation axes (Rayment *et al.*, 1992). Furthermore, their subunits pack together to form the dimers in a fashion similar, although not identical, to each other and to that predicted for the *C. vinosum* HiPIP at low temperature (Dunham *et al.*, 1991). Examination of the *E. vacuolata* HiPIP unit cell, which contains only one molecule in the asymmetric unit, reveals that the *E. vacuolata* molecules also pack as dimers but this time with their molecular 2-fold rotation axes coincident with the crystallographic dyads lying parallel along the *b* direction. This type of packing arrangement is shown in Figure 9. The interface between the two subunits constituting the *E. vacuolata* dimer is formed by loops delineated by Ala 10–Glu 15, His 25–Glu 29, and Thr 66–Ala 70. In the *R. tenuis* and *E. halophila* HiPIP dimers, the iron–sulfur centers are approximately 10.9 and 13.4 Å apart, respectively, as measured from S4 of the clusters. In the *E. vacuolata* HiPIP dimer, these inorganic sulfurs are approximately 17.5 Å apart. It is important to note, however, that while the same general face of each of these proteins is involved in subunit–subunit interactions, the exact orientation of the monomers constituting these dimers is different. It is possible that the dimeric nature of the HiPIPs, as observed in the unit cells for the *E. vacuolata, E. halophila*, and *R. tenuis* molecules, is simply a result of the fact that one side of the molecule is relatively hydrophobic and that the crystals are grown under very high ionic strength conditions. However, it is also possible that this relatively hydrophobic face, which consistently forms the "monomer–monomer" interfaces seen in the crystalline lattices, may be involved in the physiological interactions between HiPIPs and their respective redox partners.

In recent years it has become apparent that three-dimensional structure is more highly conserved than is amino acid sequence and that structural homology is often observed where there is little or no apparent sequence similarity. As can be seen in Figure 10, the amino acid sequence homology for the four HiPIPs discussed in this paper is approximately 28%, and yet the structural identity is nearly 85% as defined below. It was anticipated that the *E. vacuolata* (isoform-II) protein would be more structurally similar to the *E. halophila* (isoform-I) molecule than to other HiPIPs because of biochemical similarities. It was therefore surprising that the N-terminal region of the *E. vacuolata* HiPIP superimposed perfectly onto the *C. vinosum* molecule but was quite different from the *E. halophila* protein. The reason for this apparent contradiction is that insertions and deletions disrupt the localized folding of the polypeptide chain. A four-residue deletion near the N-terminus of the *E. halophila* HiPIP is responsible for this difference.

Where insertions and deletions exist, it is perhaps appropriate to consider ϕ,ψ angles as well as interatomic distances to assess structural similarity. The algorithm of Rossmann and Argos (1975), while exceedingly helpful, considers only distance criteria. We have visually aligned the X-ray structures of the HiPIPs by the additional criterion of dihedral angles in order to arrive at a more realistic measure of relatedness. Where the dihedral angles are similar but the α-carbon distances relatively large, the amino acid residues are considered to be homologous. On the other hand, when the α-carbon distances are small but the dihedral angles are dissimilar, the amino acid residues are judged to be nonhomologous. By these criteria, it is possible to locate the insertions and deletions in the HiPIPs much more precisely than in the past, and the apparent structural identities are somewhat larger than originally believed. The pattern of insertions and deletions, the overall structural identity, and the percentage amino acid sequence identity all indicate that the *E. vacuolata* (isoform-II) HiPIP is intermediate between the *C. vinosum* and the *E. halophila* (isoform-I) HiPIP. This example clearly illustrates that it is not possible to accurately model amino acid sequence substitutions in a protein of unknown structure onto that of a known structure when insertions and deletions are present. For this reason, it is necessary to solve the structures of a wide range of HiPIPs in order to determine what is conserved and therefore what is likely to be biochem-

FIGURE 10: Amino acid sequence alignments of the HiPIPs based on three-dimensional structures. Amino acid sequences for the *C. vinosum*, *E. vacuolata* (isoform-II), *E. halophila* (isoform-I), and the *R. tenuis* HiPIPs are labeled (A), (B), (C), and (D), respectively. The lines, labeled a–d, under each amino acid sequence (A–D) represent pairwise comparisons of the α-carbon positions of each test structure (a–d) with each reference structure (A–D). Lowercase letters refer to the same species as uppercase letters. Note that only half of the comparisons are unique (i.e., A–b is the same as B–a). The consensus represents that portion of the structure where all of the lines are the same as shown at the bottom of the figure (con.). The consensus is expected to shrink as additional structures are determined.

ically important rather than to rely on amino acid sequence comparisons alone. It is anticipated that the study of the molecular motifs of additional HiPIPs, as well as the construction of site-directed mutants, will be necessary before a detailed structural understanding of redox potential modulation in this class of proteins can be achieved.

REFERENCES

Adman, E. T., Sieker, L. C., & Jensen, L. H. (1973) *J. Biol. Chem. 248*, 3987–3996.

Adman, E. T., Sieker, L. C., & Jensen, L. H. (1976) *J. Biol. Chem. 251*, 3801–3806.

Ambler, R. P., Meyer, T. E., & Kamen, M. D. (1994) *Arch. Biochem. Biophys.* (submitted).

Backes, G., Mino, Y., Loehr, T. M., Meyer, T. E., Cusanovich, M. A., Sweeney, W. V., Adman, E. T., & Sanders-Loehr, J. (1991) *J. Am. Chem. Soc. 113*, 2055–2064.

Banci, L., Bertini, I., Capozzi, F., Carloni, P., Ciurli, S., Luchinat, C., & Piccioli, M. (1993) *J. Am. Chem. Soc. 115*, 3431–3440.

Bartsch, R. G. (1978) *Methods Enzymol. 53*, 329–340.

Beinert, H. (1990) *FASEB J. 4*, 2483–2491.

Bernstein, F. C., Koetzle, T. F., Williams, G. J. B., Meyer, E. F., Jr., Brice, M. D., Rogers, J. R., Kennard, O., Shimanouchi, T., & Tasumi, M. (1977) *J. Mol. Biol. 112*, 535–542.

Breiter, D. R., Meyer, T. E., Rayment, I., & Holden, H. M. (1991) *J. Biol. Chem. 266*, 18660–18667.

Carter, C. W., Jr., Kraut, J., Freer, S. T., Alden, R. A., Sieker, L. C., Adman, E., & Jensen, L. H. (1972) *Proc. Natl. Acad. Sci. U.S.A. 69*, 3526–3529.

Carter, C. W., Jr., Kraut, J., Freer, S. T., Xuong, N.-H., Alden, R. A., & Bartsch, R. G. (1974) *J. Biol. Chem. 249*, 4212–4225.

Chu, C. T.-W., Lo, F. Y.-K., & Dahl, L. F. (1982) *J. Am. Chem. Soc. 104*, 3409–3422.

Crowther, R. A. (1972) *The Molecular Replacement Method* (Rossmann, M. G., Ed.) pp 173–178, Gordon and Breach, New York.

Dunham, W. R., Hagen, W. R., Fee, J. A., Sands, R. H., Dunbar, J. B., & Humblet, C. (1991) *Biochim. Biophys. Acta. 1079*, 253–262.

Fitzgerald, P. M. D. (1988) *J. Appl. Crystallogr. 21*, 273–278.

Fox, G. C., & Holmes, K. C. (1966) *Acta Crystallogr. 20*, 886–891.

Freer, S. T., Alden, R. A., Carter, C. W., Jr., & Kraut, J. (1975) *J. Biol. Chem. 250*, 46–54.

Herskovitz, T., Averill, B. A., Holm, R. H., Ibers, J. A., Phillips, W. D., & Weiher, J. F. (1972) *Proc. Natl. Acad. Sci. U.S.A. 69*, 2437–2441.

Jones, T. A. (1985) *Methods Enzymol. 115*, 157–171.

Kabsch, W. (1988a) *J. Appl. Crystallogr. 21*, 67–71.

Kabsch, W. (1988b) *J. Appl. Crystallogr. 21*, 916–924.

Kraulis, P. J. (1991) *J. Appl. Crystallogr. 24*, 946–950.

Kusche, W. H., & Truper, H. G. (1984) *Arch. Microbiol. 137*, 266–271.

Langen, R., Jensen, G. M., Jacob, U., Stephens, P. J., & Warshel, A. (1992) *J. Biol. Chem. 267*, 25625–25627.

Matthews, B. W. (1968) *J. Mol. Biol. 33*, 491–497.

Meyer, T. E., Przysiecki, C. T., Watkins, J. A., Bhattacharyya, A., Simondsen, R. P., Cusanovich, M. A., & Tollin, G. (1983) *Proc. Natl. Acad. Sci. U.S.A. 80*, 6740–6744.

Meyer, T. E., Fitch, J., Bartsch, R. G., Tollin, D., & Cusanovich, M. A. (1990) *Biochim. Biophys. Acta 1017*, 118–124.

Rayment, I., Johnson, J. E., & Suck, D. (1977) *J. Appl. Crystallogr. 10*, 365.

Rayment, I., Wesenberg, G., Meyer, T. E., Cusanovich, M. A., & Holden, H. M. (1992) *J. Mol. Biol. 228*, 672–686.

Rossmann, M. G., & Argos, P. (1975) *J. Biol. Chem. 250*, 7525–7532.

Stombaugh, N. A., Sundquist, J. E., Burris, R. H., & Orme-Johnson, W. H. (1976) *Biochemistry, 15*, 2633–2641.

Thaller, C., Weaver, L. H., Eichele, G., Wilson, E., Karlsson, R., & Jansonius, J. N. (1981) *J. Mol. Biol. 147*, 465–469.

Thaller, C., Eichele, G., Weaver, L. H., Wilson, E., Karlsson, R., & Jansonius, J. N. (1985) *Methods Enzymol. 114*, 132–135.

Tronrud, D. E., Ten Eyck, L. F., & Matthews, B. W. (1987) *Acta Crystallogr. A43*, 489–501.